The Rebirth of the Current Source Inverter: Advantages for Aerospace Motor Design

Vincenzo Madonna, Giovanni Migliazza, Paolo Giangrande, Emilio Lorenzani, Giampaolo Buticchi and Michael Galea

University of Nottingham
UK | CHINA | MALAYSIA

University of Nottingham Ningbo China, 199 Taikang East Road, Ningbo, 315100, Zhejiang, China.

First published 2019

University of Nottingham
UK | CHINA | MALAYSIA

The rebirth of the Current Source Inverter: advantages for aerospace motor design

Vincenzo Madonna, Giovanni Migliazza, Paolo Giangrande, Emilio Lorenzani, Giampaolo Buticchi and Michael Galea

Published in:
IEEE Industrial Electronics Magazine, vol. 13, no. 4, pp. 65-76, Dec. 2019.

Document Version:
Accepted Author manuscript, peer reviewed, unedited version

Introduction

It is well-known and widely accepted that today the world of electrical drives is dominated by the Voltage Source Inverter (VSI). Its success is probably due to its simplicity, the general availability of voltage sources and the high efficiency that it can achieve. This popularity has in turn also influenced how the semiconductor industry has developed, where a focus on devices tailored for VSI usage has been the norm in the last years. Thus, products such as depletion devices (normally off) and without reverse voltage blocking capability have seen widespread marketing and use.

On the other hand, the current source inverter (CSI), while never very popular, has in the last two decades, been pushed even more into obscurity. Based on the common, pre- wide bandgap era technologies and topologies, then applications and scenarios where CSIs would give an inherent advantage are few and far between. This trend is today however changing. The quest for higher efficiencies and power density, combined with new technological developments is 'opening' up the playing field to CSIs. The CSI's inherent characteristics of intrinsic voltage boost, a low output voltage THD and the absence of electrolytic capacitors are all extremely important benefits that, if taken advantage of and designed for, can result in a resurrection of the CSI in the very near future. It is perceived that certain niche applications can benefit greatly from the development and implementation of CSIs. For example, any high speed drive that is limited with a low voltage source, e.g. for transport applications, will be an ideal breeding ground for the next generation of CSI converters.

The paper therefore presents a study, whose main aim is to investigate and define the real potential of CSI-based electrical drives in the context of future transport applications. If one was to consider the main aerospace requirements, namely power density, efficiency and reliability, then the CSI's lack of DC link capacitors represents a promising solution for any future aircraft. To reach this aim, a case study for a real application is developed. A variable speed drive (VSD) for the environmental control system (ECS) unit of a single aisle commercial aircraft is designed. This is done using both a CSI and a VSI. The two configurations are then analysed and compared, showing how the converter choice can strongly impact the machine/drive performances.

Setting the context

A main aim of the more electric aircraft (MEA) concept is the reduction of jet fuel consumption and therefore less emissions. A common school of thought in this area is to try to achieve this by working towards ever more efficient aero engines, with the ultimate aim of a completely bleed-less

engine scenario. Thus, all the air being compressed by the engines will be used for propulsion, without having to also feed all the secondary systems onboard the aircraft.

However, in modern commercial aviation history, this aspect has never been fully implemented. The traditional limitations on the amount of electrical power that is typically generated on-board was always in contrast with the actual amounts of power that are required to operate all the secondary systems. Examples of huge power drainers include the aircraft ECS and de-icing systems. The absolute values of the power required by these systems were always simply too much. However, the introduction into the market of the Boeing 787 in 2011 represented a paradigm-change in the aerospace community [1]. With its total installed power of 1 MVA (main generators only), the B787 was the first commercial platform to be considered a really "more electric aircraft" (MEA) [2]. This "power anomaly" is easily spotted in Figure 1, where the (main) generators power is plotted against the engines take-off thrust for various commercial aircraft. This step-change in the value of power generated on-board the B787 is due to two main aircraft design choices, namely that the cabin's ECS and the aircraft's de-icing system are both electrically controlled. The B787's composites-based body allows for much higher levels of cabin pressurisation and this therefore underpins and justifies the use of electrically controlled ECSs. It is also important to note that an added advantage of these choices is that the B787 can then comprise a completely bleed-less engine, i.e. no air is needed to be bled from the turbofans to actuate the secondary systems. For completeness, Figure 2 and Figure 3 show a schematisation of conventional and a no-bleed engine architectures respectively.

Thus, the B787 is the first commercial aircraft to have a fully electrically controlled ECS. Today's implementation comprises a VSD that makes use of a VSI configuration. The system's electrical machines (EMs) are fed by a PEC to precisely control the speed and thus allowing optimal and efficient operations. In the B787, the same PEC is also used for engine-starting purposes, operating the variable speed starter/generator in motoring mode [3]. The VSI-based drive has been shown to be extremely well-suited to the application at hand. However, as shown later in this work, it is the authors' opinion that considering the nature of the application, then even better performance can be achieved when a machine with higher voltage is employed for the design. Higher voltage for the machine would imply either a VSI with dc-dc front-end with a large capacitive dc-link to step up the bus voltage. However, with a CSI solution, this could be achieved smoothly.

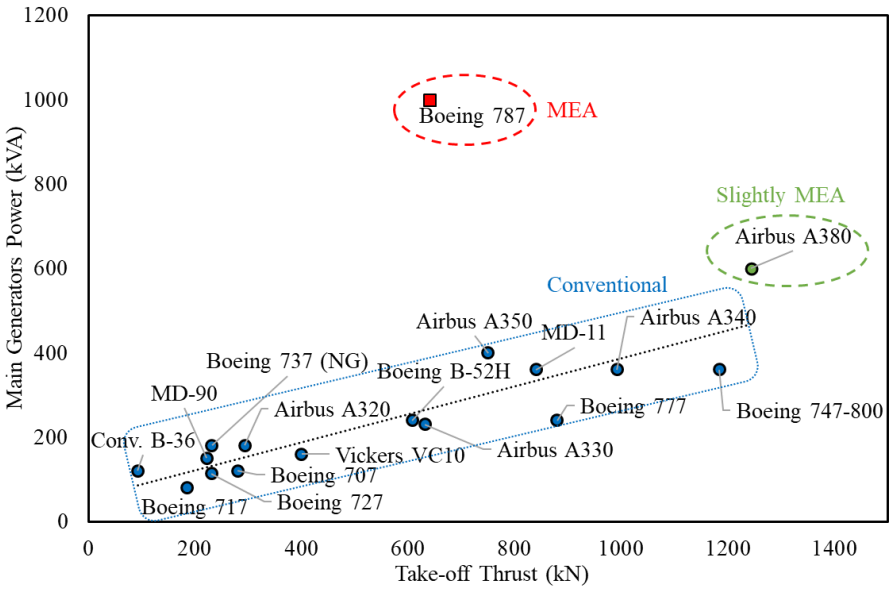

Figure 1 – Main generators power vs. take-off thrust for various aircraft.

This article will therefore develop a comparative study that pits a CSI drive (preferred to the boost converter + VSI solution due to the reduced capacitance required) against the traditional VSI drive for the control of a permanent magnet synchronous machine (PMSM) powering/driving an ECS compressor. Alternatively, Z-source or quasi Z-source Inverter topologies [4, 5] can be used to step-up the input DC link voltage, however the commutations are similar to those of a conventional VSI. This means that, for an EM fed by a Z-source inverter topology, the insulation must be designed to withstand PWM-modulated pulses. Additionally, if wide bandgap devices are used, the stress on the insulation is further enhanced, compromising the overall drive reliability.

The advantages of a drive based on the CSI topology against the more conventional VSI in the context of a low voltage, high speed application are derived. These will then be used to develop a case in support for the authors' belief that the CSI drive does have a potential future. It is true that it is a future that probably won't be as widely applicable as that of the VSI drive as we know it today, however with this work the authors hope to show that for particular cases, the CSI drive does win.

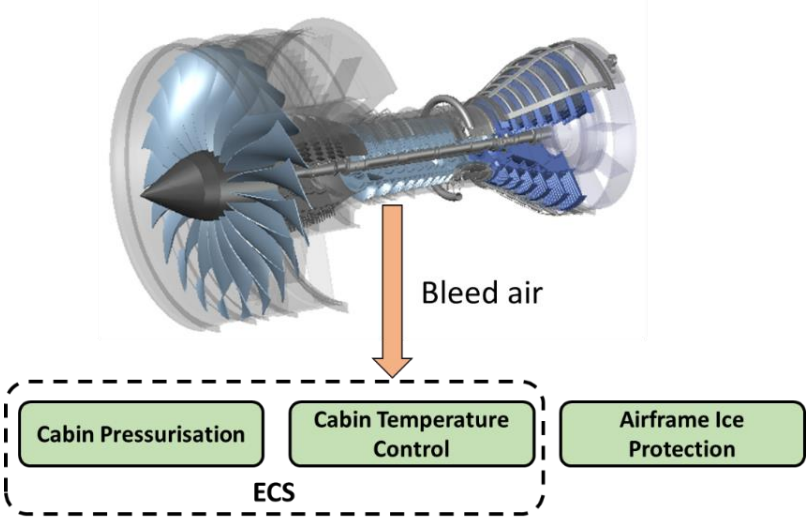

Figure 2 – Conventional turbofan engine with bleed air extraction for powering secondary sub-systems.

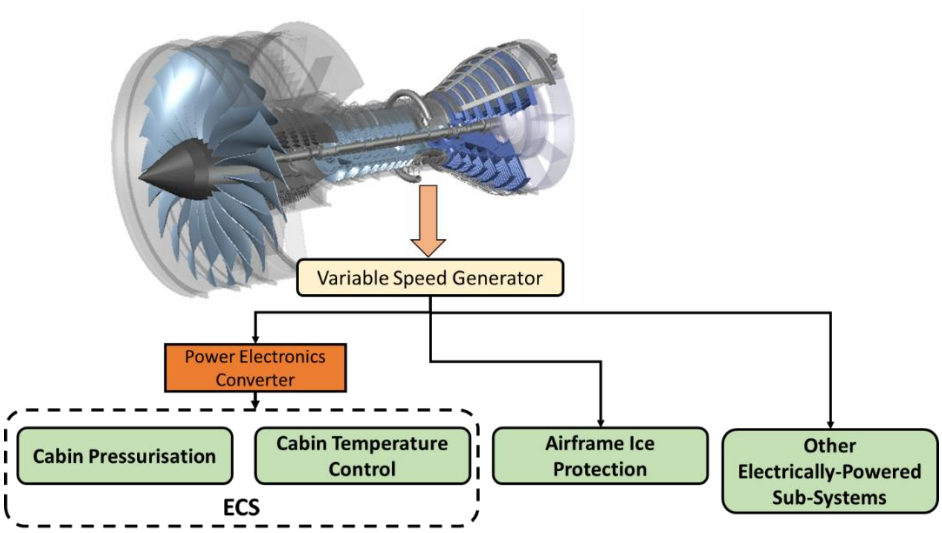

Figure 3 – No-bleed engine where secondary systems are electrically-powered.

The Current Source Inverter

For CSI systems, one of the first related patents was presented by L. W. PARKER in 1939 [6]. The intrinsic voltage boost capability of this first topology, named Direct Current voltage booster, was at that time primarily used for driving the then so-common vacuum tubes, that performed the required switching operations. The subsequent designs made use of Silicon Controlled Rectifier, that exhibited the reverse voltage blocking capability could be controlled both in turn-on and turn-off.

The development of semiconductor technology and the large availability of Insulated Gate Bipolar Transistors (IGBT) cleared the way for the VSI to become the dominant technology in electrical drives. The high voltage blocking capability, the ease of driving and the very good conduction and switching performance made very easy the realization of a VSD with just 6 IGBT and 6 diodes. The characteristic of the IGBT to be in a blocking state when the gate is not energized constituted a safety element that simplified the protection system: during a fault, all devices could be de-energized, stopping the power flow.

Realizing a CSI with devices highly optimized for VSI application proved to be a hard task, since the need of adding a series diode to the IGBT to ensure the reverse blocking capability, practically doubling the conduction losses. Due to the presence of an inductive dc link, during a faulty situation, it must be ensured that the inductor current has a free-wheeling path. Even when the power flow stops, the devices must be switched on to avoid the inductor open-circuit and the consequent converter destruction. Additionally, making the CSI bidirectional would imply doubling the number of active devices, making the adoption from industry virtually impossible.

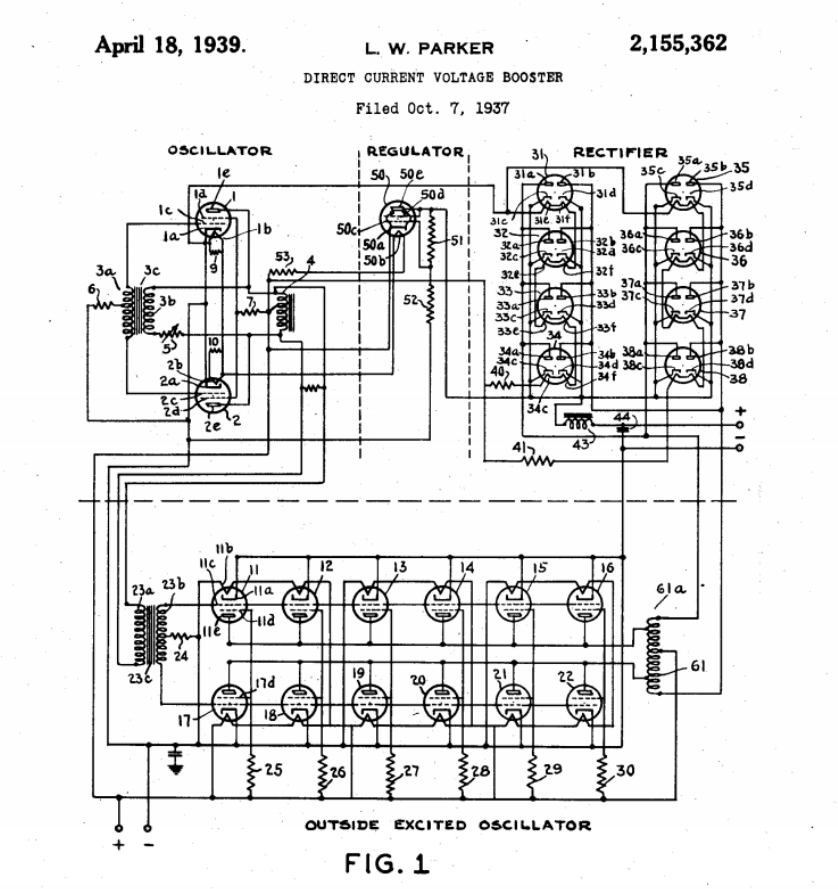

Figure 4 – First patent of a topology based on CSI idea [6].

The most distinguishing feature of a CSI is that its output voltage is higher than its input voltage. Whereas the VSI topology "slices" the input voltage, behaving as a buck converter (the output voltage is lower than Input voltage), the CSI converter behaves as a boost converter. Also, a CSI requires a current source. This is usually provided by a pre-stage sub-system that operates in continuous conduction mode, which of course deteriorates significantly the system's efficiency.

Table 1 – Topology Comparison.

Characteristic	VSI	CSI
Output capability	Buck	Boost
Input Filter	Capacitor	Inductor
Leg Switching Behaviour	Dead Time	Overlap time
Output Current THD	Low	Low
Output Voltage THD	High	Low

An input inductor is required for a CSI. For a long time, the frequency limitation of the semiconductor devices also implied that in order to have an almost constant current, the input inductor be of quite an elevated value, resulting in bulky and heavy input inductors. A qualitative comparison of the features of classical VSIs and classical CSIs is shown in Table I.

From this initial description, it seems that the adoption of the CSI for a VSD is basically impossible, with the boosting capability the only superior point to the VSI. But technology can always tip the scales…

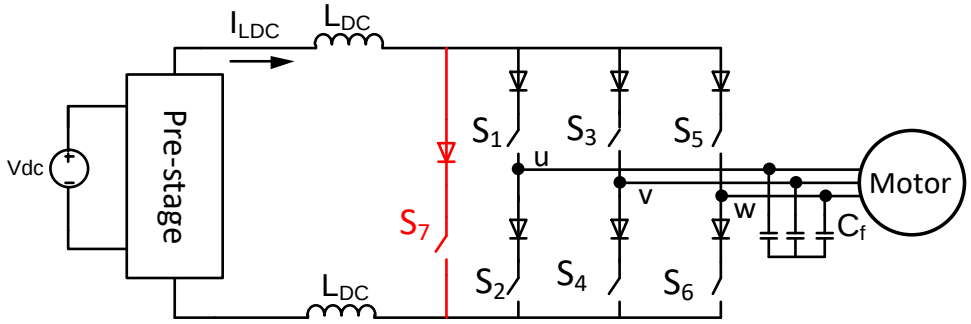

Figure 5 –Current Source Inverter topology (black lines) with the addition of device S7 (red lines) to improve converter performance.

Moving forward

Today, new and more powerful technologies are however levelling the playing field more than ever before. New wide bandgap devices such as Silicon Carbide products allow for much higher switching frequencies to be operated in, while at the same time reducing conduction losses. The use of semiconductor devices, such as IGBT-RBs (i.e IXRP15N120), Dual-Gate GaN Bidirectional Switches [7] or SiC Devices (i.e C2M0025120D) can result in reducing the dimension of the input inductor with obvious benefits in terms of power density. Advances in control methodologies is another enabler for the re-birth of CSI drives. The use of an additional device S7 (shown in red in Figure 5) with a suitable Space Vector Modulation (SVM) [8] can reduce conduction losses, the THD of output currents and also the ground leakage current. The latter is particularly important for aerospace applications where reliability and fail-safe systems are essential requirements. Various effective

solutions to reduce ground leakage currents can be migrated, through CSI technologies, to the aerospace field from the energy sector, e.g. photovoltaic applications, e.g. [9].

Considering all this, it is therefore very probable that customised designs can result in CSI systems that can fairly compete with VSIs. Once the differences in terms of efficiency due to the optimized devices and topology would allow to obtain very good result, its inherent voltage boost capability would make it ideal for high speed operations where only a relative low-voltage source is available.

The VSI plus dc-dc converter would still suffer from the need of a capacitive dc link and possibly an output filter (i.e. on the AC side of the inverter) due to the high voltage THD. It is also important to put in evidence that the 6 transistors of the main CSI bridge are subjected to a limited voltage swing during commutations respect to the VSI case. This voltage swing varies during time following output line-to-line voltages, in which amplitude follow obviously the machine speed. The use of the additional device S7 allows also to obtain Zero Current Commutations for the 6 transistors of the main bridge.

Summarizing the CSI excellent output voltage waveform implies lower stresses on the insulation systems of the converter itself but also on the insulation systems of the EM, making it the definite winner of the competition.

A Case-Study: High-Speed Electrical Drive Design

Background

This section aims at analysing the benefits arising from the implementation of a power converter with boost capability, as the CSI converter, for controlling an electrically-powered ECS compressor. The specifications reflect the actual needs for an aerospace electrical drive system to power a compressor.

The system is a classical VSD, comprising a machine, a PEC and a control platform. The main design requirements and constraints for the complete drive are listed in Table 2. The selected voltage level (i.e. 270 V) is conventionally adopted for supplying VSDs in modern aircraft (e.g. B787, A350 and A380). This voltage level is obtained from the main 115/230 V AC variable frequency distribution, through the use of an auto-transformer rectifier unit [2, 10].

Table 2 - Main design requirements for the ECS compressor drive.

Parameter	Quantity
DC link voltage	270 V
Rated power	25 kW
Maximum speed	25000 rpm
Max EMF THD	5 %
Efficiency	>95%
Cooling method	Forced liquid (water jacket)
Available flow rate	6 L/min
Maximum hot-spot	150 °C +/- 10°C

The project's objective was to preliminary identify the optimal system-level configuration, including the identification and design of the PEC and of the EM. In light of this paper, three main configurations comprising three different high speed PMSM designs, were proposed and investigated. The three configurations are roughly categorised as

1) Machine 1, fed by a VSI

2) Machine 2, fed by a VSI
3) Machine 3, fed by a CSI

The three EMs are "tailored" to the available converter. That is, for each converter topology, the most optimised EM able to satisfy/meet the design requirement is proposed. It is worth remarking that the previously-mentioned VSI topologies with boost capability are not analysed in this study. Indeed, the boost capability comes at the cost of a) increased component counts and related losses, b) increased drive complexity and c) detrimental effect on the EM insulation, given by the high voltage, short rise-time PWM modulated pulses.

Development of EMs

The design of high-speed EMs for aerospace is a challenging task and should be tackled through a multi-disciplinary approach [11]. Some of the various disciplines involved in the design procedure of such machines are illustrated in Figure 6. Alongside to improved thermal management techniques [12, 13] and electromagnetic computational tools, the design of high-speed EMs requires mechanical expertise for sizing of the rotor structure [11, 14, 15]. The stiffness and geometrical dimensions of the shaft must be carefully chosen for avoiding resonances, which might severely compromise the whole rotor structure, causing the machine outage. At the same time, the structural integrity of the rotor must be guaranteed in any operating situation, by e.g. using high strength retaining sleeves for the containment of permanent magnets (PMs) under elevated centrifugal forces. Last (but not least) the EMs for aerospace are commonly employed in safety-critical applications, where a machine failure might endanger human life and/or cause extensive economical loss. It is then required that such EMs operate with an enhanced reliability level with respect to ground-based counterparts (e.g. home appliances, industrial and automotive). Therefore, aerospace EMs' reliability have to be assessed via physics of failure – based lifetime prediction models [16, 17] starting from an early design stage.

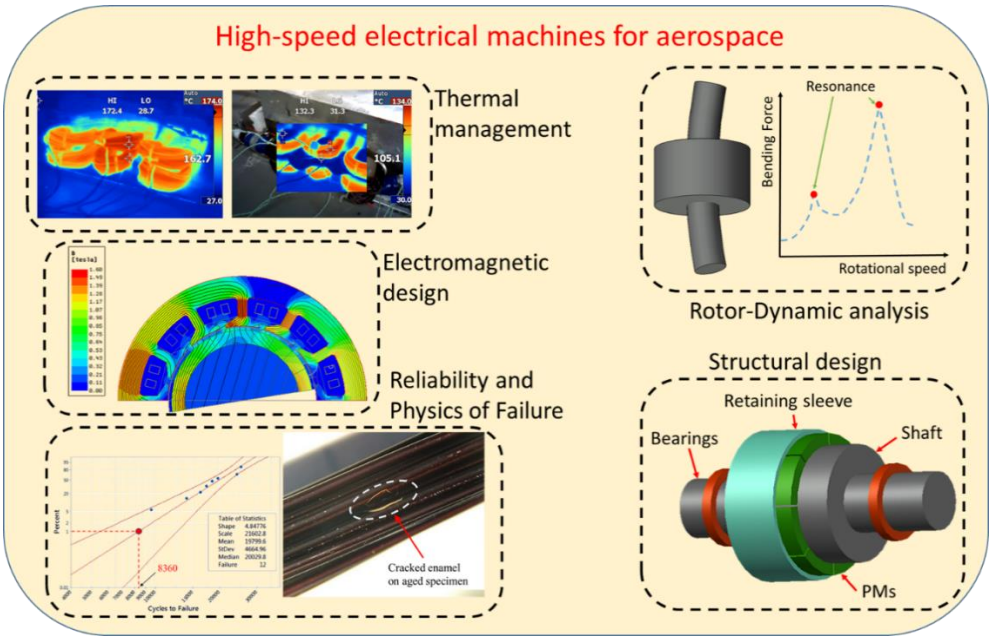

Figure 6 – Multiphysics aspects involved in the design of high-speed EMs for aerospace.

Machine 1: VSI-fed without flux weakening operations

The first machine is designed to be VSI-fed and operated at a base speed of 25000 rpm. Hence, flux weakening capabilities are not required and, therefore, a PMSM with surface mounted PMs is chosen (i.e. ≈unitary rotor saliency ratio).

Given the relatively high rotational speed (i.e. 25000 rpm), the aspect ratio (i.e. ratio between axial length L and stator bore diameter D) is kept ≈1. This choice moves the critical speeds of the rotor (i.e. resonance frequencies) above the EM operating range [14].

In order to maintain a relatively low fundamental frequency, despite the high-speed application, a 2-pole design is chosen. The THD of the back electromotive force (BEMF) is reduced by suppressing 5th and 7th harmonic fields. This is done by choosing the slot number *Q* equal to 12 and by adopting a double layer winding shortened by one slot pitch (i.e. the coil pitch calculated as *Q/2p-1* is equal to 5).

The surface mounted PMs are directly glued on the rotor shaft (i.e. no lamination) and a carbon fibre retaining sleeve is wrapped over them, in order to avoid their detachment, due to the centrifugal forces [15]. The PM thickness is appropriately chosen for preventing the demagnetization risk due to both short-circuits at maximum speed and high operating temperatures. The PMs span is equal to 1 (i.e. 180 eDeg), bringing a continuous PMs arc over the rotor (shaft) surface, and thus minimizing single stress-points over the retaining sleeve [15]. For cutting-down the rotor losses caused by eddy effect, the PMs are axially and radially segmented [18]. Additionally, they are parallel magnetised for having a sinusoidal airgap magnetic field and improving (reducing) the BEMF THD and torque ripple. The resulting machine geometry (i.e. radial cross-section) and winding layout are shown in Figure 7.a, while its main geometrical dimensions are given in Table 3. The electrical parameters obtained from the FE simulations are listed in Table 4.

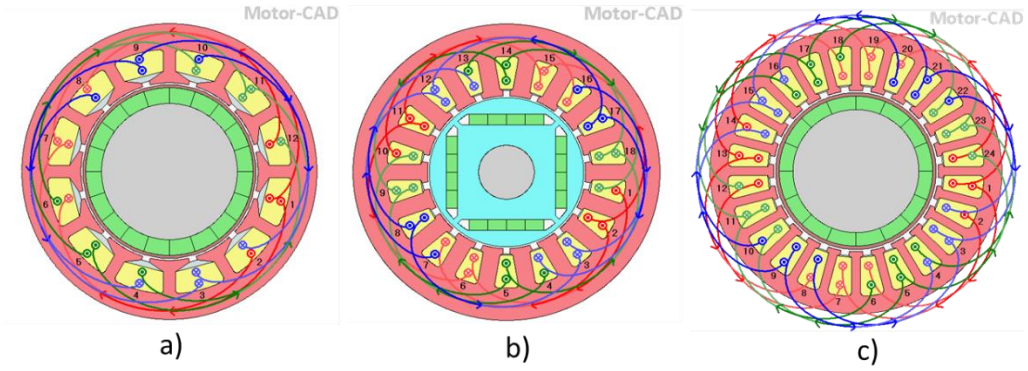

Figure 7 – Geometry and winding layout for the three designed machines: a) Machine 1; b) Machine 2; c) Machine 3.

Machine 2: VSI-fed with flux weakening operations

Machine 2 is designed to be VSI-fed with flux weakening capabilities. Therefore, the base speed of 10000 rpm and the maximum speed of 25000 rpm are fixed at the design stage. For providing the EM with this capability, an anisotropic rotor structure is chosen by selecting an internal PM configuration. This arrangement guarantees an excellent anisotropy (between d and q magnetic axes), improving the torque-producing capability at high speed. However, the rotor structural integrity must be evaluated for the whole speed range. In fact, in this case, the PMs are “buried” inside the rotor core and retained trough brittle lamination bridges without any sleeve or additional containment system. A structural FE analysis at maximum speed (see Figure 8) is required for

verifying that the rotor lamination stress is below the yield strength of the material (with some 20-30% safety margin.

A 18 slot, 4 pole design is selected after a trade-off analysis as shown in Figure 7.b and reported in Table 3 where the main geometrical dimensions are listed. The flux weakening control strategy, necessary for operating the machine at 25000 rpm is shown in Figure 9, while the FE electromagnetic analysis results are summarised in Table 4.

Because Machine 2 operates with $I_d \neq 0$, care must be taken in order to avoid loss of control at high rotational speed. Indeed, this working condition, defined uncontrolled generator operation, might develop a voltage level at the machine terminals well above the DC link voltage which compromises the electrical safety and, if a proper braking circuit is not provided (at converter level), can over-charge the DC link capacitor with severe consequences.

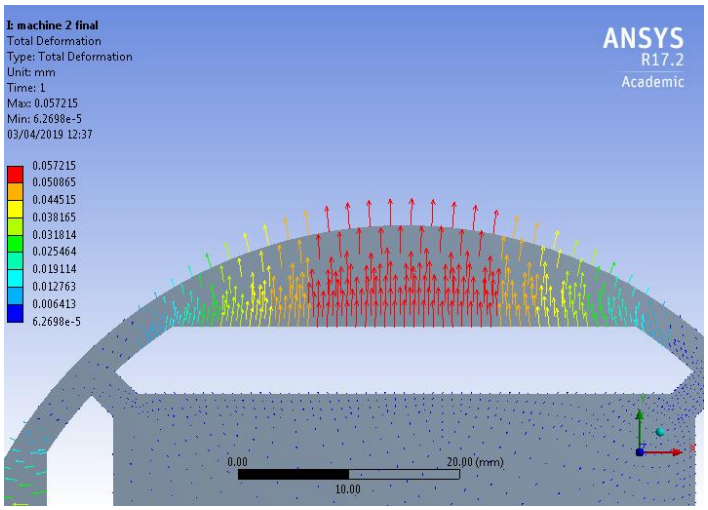

Figure 8 – Structural FE analysis for a internal PM rotor: total deformation at high speed operations (25000 rpm).

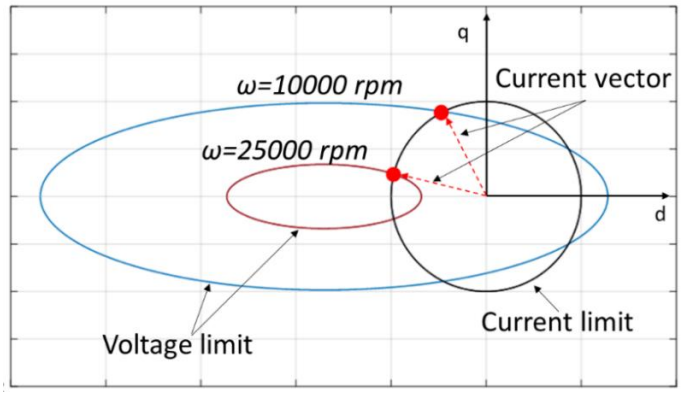

Figure 9 – Field weakening control strategy.

Machine 3: CSI-fed

Differently from Machine 1 and 2, the third machine is developed to be fed through the CSI converter topology presented in the previous Section. One of the main advantages of this drive topology are the benefits deriving from the voltage boost capability of the CSI. A higher per-phase voltage gives to the EM designer more freedom in the slot/pole combination choice, as well as in the selection of the winding layout. Further, because in CSI-fed EMs the terminals voltage is quasi-sinusoidal, the insulation system is less stressed than in VSI drives. In fact, the turn-to-turn insulation is only subject to a portion of the total phase voltage (inversely proportional to the number of turns

per phase). On the other hand, in VSI drives (and in particular those adopting wide-bandgap SiC MOSFETS) the turn-to-turn insulation might experience voltage levels as high as two times the DC-link voltage [19]. Thus, a machine fed by a CSI converter can rely on lower grade (i.e. thinner) interturn insulation, enhancing the slot copper fill factor, and guaranteeing a higher power density [20].

For Machine 3, a 24 slot 4 pole configuration is selected after an analytical trade-off study. The PMs form a continuous arc over the rotor external circumference, and they are radially and axially segmented. The main design parameters of Machine 3 are listed in Table 3, while the geometry and winding layout are shown in Figure 7.c. The PMs are directly glued on the shaft and they are retained by a carbon fiber sleeve, similarly to Machine 1. A particular design solution, consisting in the PMs skewing by 15 mechanical degrees (i.e. 5 axial segments displaced by 3 degrees each) allows to minimise the torque ripple to 1.5 %. This expedient (i.e. PMs skewing) is easily implemented in surface mounted PMSMs, whereas it leads to significant manufacturing complexity in interior PM machines (i.e. Machine 2).

The full-load flux density and magnetic field lines of Machine 3 are depicted in Figure 10, while Table 4 summarizes the main findings obtained from the FE simulations. From Figure 10, it is possible to observe that Machine 3 does not operate in deep magnetic saturation, ensuring a wide overload capability.

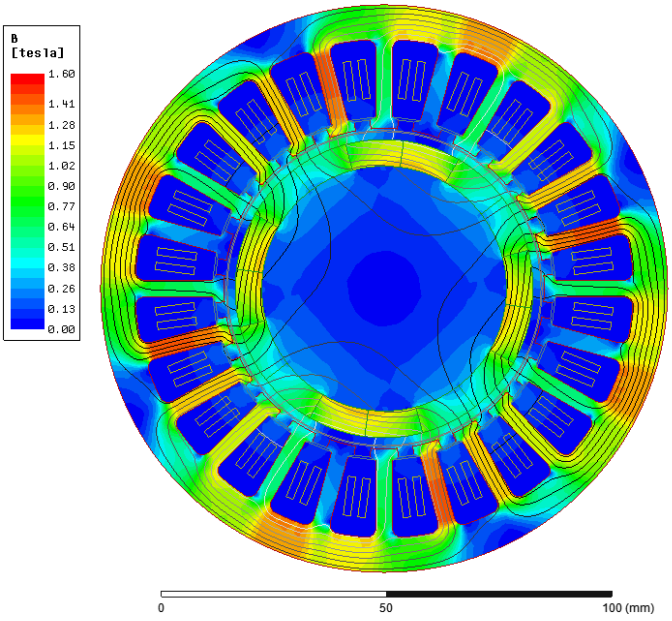

Figure 10 – Machine 3 magnetic flux density map and field lines at 25000 rpm.

Table 3 – Main design parameters for the three considered machines.

Parameter	Machine 1	Machine 2	Machine 3
Pole pairs, p	1	2	2
Slot number, Q	12	18	24
Turns per coil	5	3	5
Stator (outer) diameter, D_{out}	150 mm	155 mm	127.5 mm
Axial length, L	85 mm	98 mm	70 mm

Table 4 – Results from FE analysis for the three machines operating at 25000 rpm.

Parameter	Machine 1	Machine 2	Machine 3
BEMF THD	<1%	3.71 %	1.6 %
Phase current	111 A (rms)	114.3 A (rms)	42.55 A (rms)
Phase advance	0 deg (i.e. i_d=0)	74 deg	0 deg (i.e. i_d=0)
L_d	0.1532 mH	0.192 mH	0.48 mH
L_q	0.1532 mH	0.446 mH	0.48 mH
Self inductance	0.1269 mH	0.33 mH	0.3945 mH
Mutual inductance	-0.02738 mH	-0.12 mH	-0.09262 mH
Line to line inductance	0.3086 mH	0.91 mH	0.9742 mH
Torque constant	0.07352 Nm/A	0.07515 Nm/A	0.2064 Nm/A
BEMF constant	0.0848 Vs/rad	0.1831 Vs/rad	0.2392 Vs/rad
Fundamental freq.	416.7 Hz	833.3 Hz	833.3 Hz
Shaft torque	11.472 Nm	11.88 Nm	12.3 Nm
Torque ripple	0.1 %	7.62 %	1.5 %
Mechanical power	30 kW	31.1 kW	32.2 kW
Total losses	847.44 W	1197 W	772 W
Efficiency (at full load)	97.3 %	96.3 %	97.66 %
Power factor	0.9	0.858	0.92
Flux linkage D	49.1 mVs	51.35 mVs	68.81 mVs
Flux linkage Q	24.3 mVs	23.48 mVs	29.31 mVs

Discussion

A comparison in terms of electromagnetic performance among the three machines is presented in Figure 11. All three machines show an excellent efficiency above the required target of 95%, with the CSI version peaking over 97%. Similarly, the BEMF THD constraint is satisfied in the three presented cases, although Machine 2 is the closest one to the 5% limit. No restrictions were imposed regarding the torque ripple. However, it is interesting to note the elevated ripple level generated by Machine 2. This is mainly caused by the difficulties, from the manufacturing point of view, of skewing an interior PM rotor. The CSI-fed machine features an outstanding power density increment. In fact, the availability of a higher per-phase voltage provided by the CSI converter, with respect to the VSI one, gives more flexibility in the slot/pole combination choice, as well as in the winding layout selection. For the sake of fairness, from the theoretical point of view, the VSI topology with no flux weakening (i.e. Machine 1) could achieve the same power density level of Machine 3. Nonetheless, it would require a particular winding arrangement with two turns per coil and more than thirty parallel strands. It is then clear that such a design choice is not in line with the “design for manufacturability” approach as, generally, 10 to 15 parallel strands are the maximum practical limit for standard random wound EMs. Furthermore, an elevated number of parallel strands, combined with the relatively high speed of the PMSM might cause non-uniform current distribution in the wire bundles [21]. This, in turn, originates localised hot-spot winding temperature, which might shorten the interturn insulation lifetime and bring reliability issues.

The three machines are apprised in terms of mechanical and thermal performances in Figure 12. It is worth remarking that the stator hot-spot temperature, for the three designs, is within the range 150 °C +/- 10 °C. Nonetheless, Machine 2 is characterised by the highest rotor hot-spot temperature (i.e. 140 °C) among the solutions, since high order harmonics in the airgap magnetic field are source of eddy current losses in the PMs. The rotor stress analysis is computed via 3D FE structural simulations performed in Ansys® Workbench. The reported stress is normalised with respect to the maximum (yield) strength of the materials (i.e. retaining sleeve for Machines 1 and 3 and lamination for Machine 2). In Figure 12.b, it is clearly observable that the rotor of the two surface-mount PMSMs (i.e. Machine 1 and 3) is not subject to excessive mechanical stress when operating at high speed. On

the contrary, the peak stress in Machine 2's rotor is c.a. 85% of the lamination yield strength indicating that, for high-speed operations, surface-mount PMSMs equipped with a retaining sleeve are preferable. The first critical speed of the three rotors is analytically-calculated assuming the shaft as a supported beam, providing thus a conservative result [14]. For all the three designs, the operating speed (i.e. 25000 rpm) is well below the critical speed. Further, thanks to the low aspect ratio of Machine 3 (i.e. CSI-fed), its critical speed is c.a. 120000 rpm (i.e. more than four times the rated speed). Finally, the active weigh (i.e. excluding passive components such as housing and shaft) of the three solutions are evaluated. It is easily observable that the CSI-fed machine weights less than the other two prototypes, followed by the VSI-fed machine with no field weakening. For a better comparison, the weight breakdown is provided in Figure 13 for the three designed solutions. In this case the, weight of the shaft is included in the computation. From Figure 13, it is also possible to roughly evaluate the most economically convenient solution (despite for aerospace EMs the cost does not generally represent a critical demand). Machines 2 and 3 require less PM material with respect to Machine 1, representing then the most cost-effective designs. Further, it is interesting to observe that the retaining sleeve, which as mentioned is an essential component in high-speed surface mounted PMSMs, represents only the 1% of the total weight (for Machines 1 and 3), due to the low mass density featured by carbon fiber.

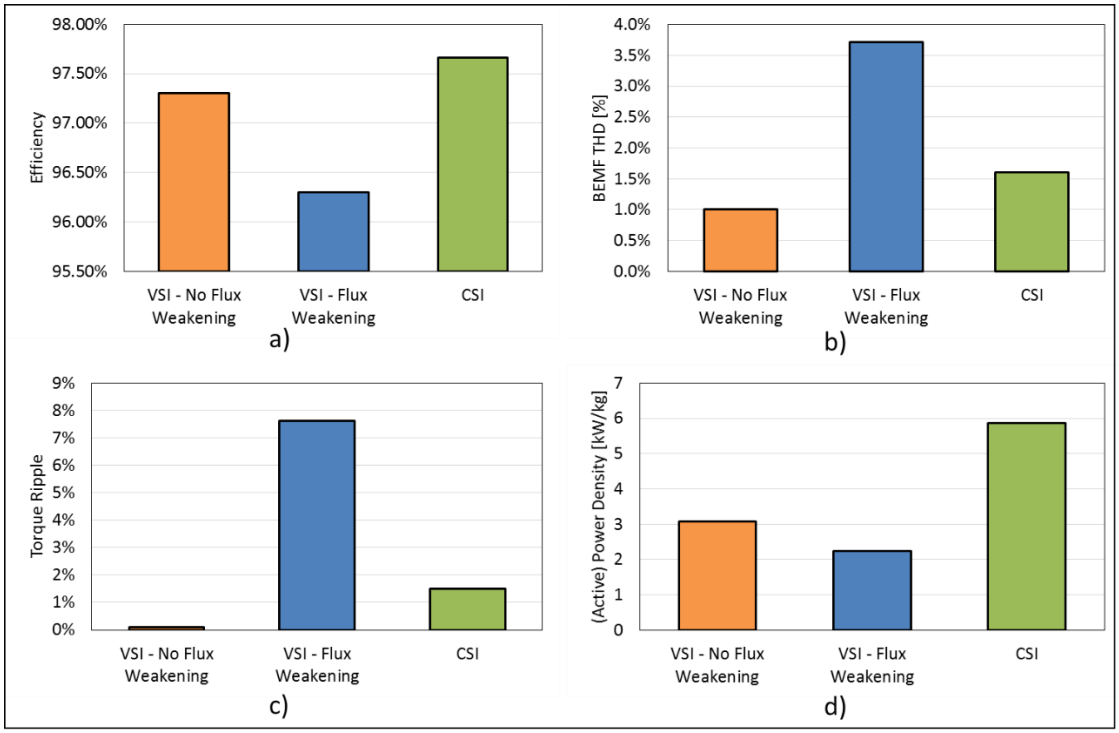

Figure 11 – Electromagnetic performance comparison among the three designed solutions: a) Efficiency; b) Back electromotive force THD; c) Torque Ripple; d) Power density considering only the active parts.

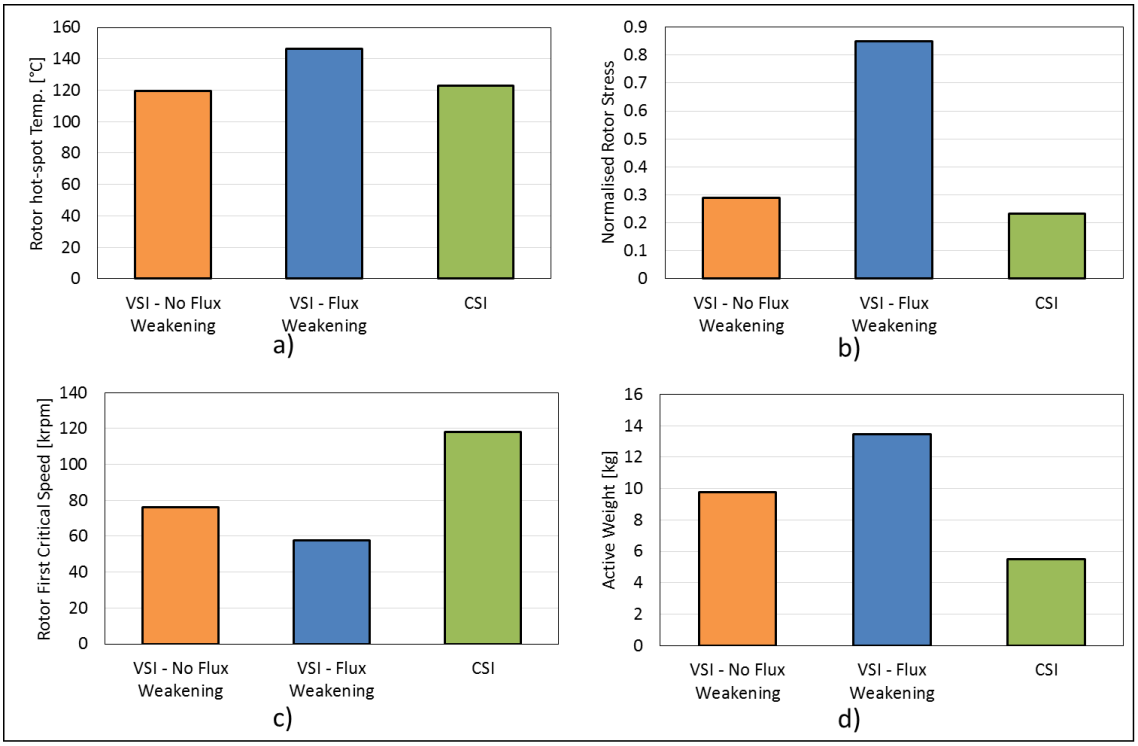

Figure 12 – Mechanical and thermal performance comparison among the three designed solutions: a) Rotor hot-spot temperature; b) Normalised rotor stress (i.e. peak stress/material's yield strength); c) Rotor first critical speed; d) Weight of active materials (i.e. excluding housing and shaft).

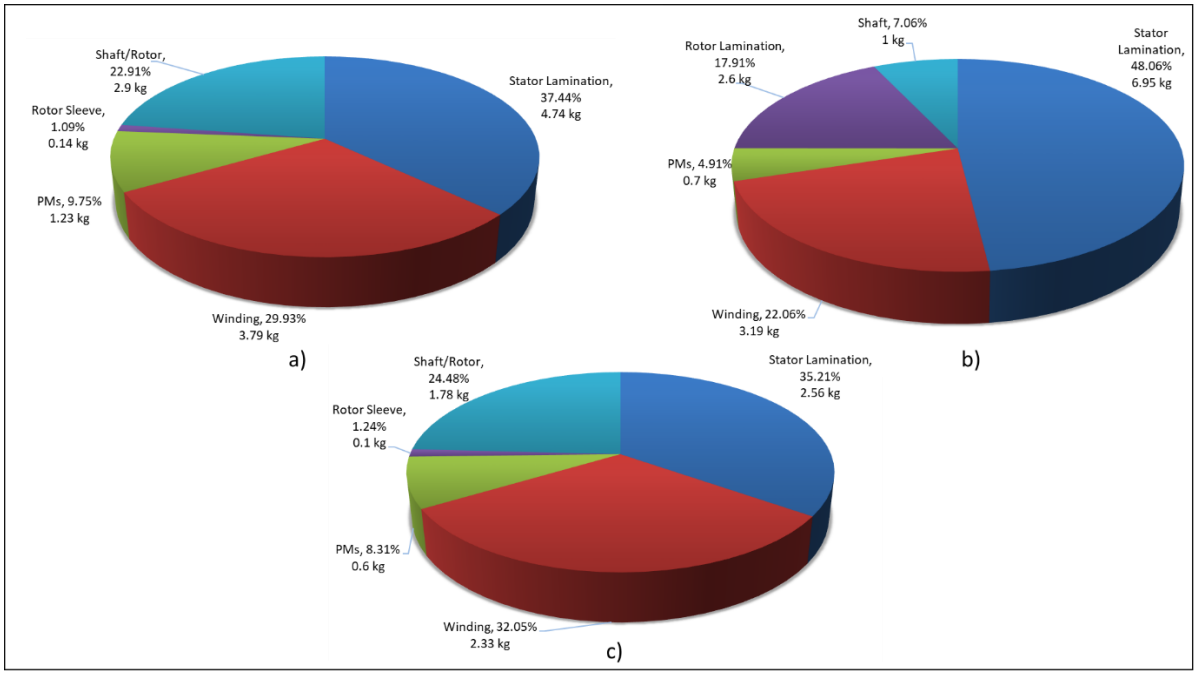

Figure 13 – Weight breakdown for the three machines: a) Machine 1 – VSI no field weakening; b) Machine 2 – VSI with field weakening; c) Machine 3 – CSI.

Conclusion and an outlook to the future

The main aim of this article is to prove how a PEC technology that has always been "brushed off" by the electric drives community, in some particular applications, might represent the optimal design choice at system level. A technology that in the past had the voltage boosting as its only benefit can

have his rebirth in a scenario where the higher voltage design of an electric machine implies benefits in the system power density. Obviously, the technology development that allows better devices with bidirectional voltage blocking capability and optimized topologies are concurrent factors that contributed to even the ground with the VSI based solutions. Once the benefits at machine level are achieved, the other characteristic of low output voltage THD and dv/dt can make the CSI as the true winner, due to the lower stress on the machine and the absence of output filter.

With an eye to the future of transportation electrification, in particular in the aerospace sector, it is necessary to "combine the efforts" between machines and power electronics designers for proposing efficient and optimised drive solutions. This work thus aims in "raising awareness" on how the converter choice can strongly influence various aspects of an EM design. The selected case-study is purposely chosen for further outlining that, when an integrated design is carried out, a system-level optimum can be achieved.

For large commercial aircraft, it is still unthinkable to replace Jet-A fuel for propulsion purposes. Current energy-storage devices represent the main bottleneck, as their energy density is still c.a. ten times less than the (minimum) required level. Nonetheless, if electrical machines are to be adopted as primary power system (i.e. propulsion), their design is not going to be a trivial process. Within 10 to 15 years, electric motors for regional aircraft propulsion, will be demanded to develop 2-5 MW of power and to be controlled by power electronics converters. Among all the "conventional" design challenges, they will need to feature an outstanding reliability, as a single failure might be catastrophic. An even higher challenge is posed by the move towards "high-voltage" systems for aerospace (1-3 kV), as this will save considerable weight and increase range and/or payload capability. Nonetheless, the harsh aerospace environment (low pressure and wide temperature range) implies a physics of failure-oriented design for the whole electric drive, which is reached by introducing reliability aspects as primary design requirement. A roadmap for electrical machines and power electronics in aerospace has been compiled in 2018 by the UK Aerospace Technology Institute and is reported in Figure 14 [22].

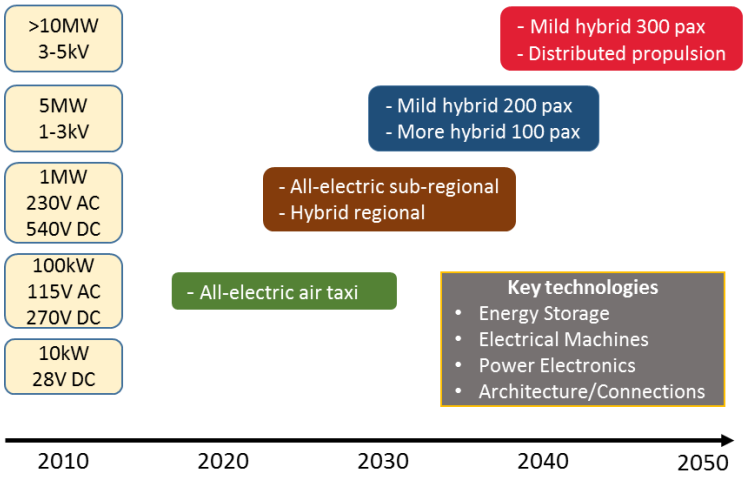

Figure 14 – Aircraft power systems/demand roadmap [22].

Several challenges will need to be tackled in the near future by the academic and industrial communities. These can represent a problem if not faced with the right approach, but at the same time they are a huge opportunity for development and prosperity. Exciting times are ahead of us.

References

[1] B. Sarlioglu and C. T. Morris, "More Electric Aircraft: Review, Challenges, and Opportunities for Commercial Transport Aircraft," *IEEE Transactions on Transportation Electrification,* vol. 1, pp. 54-64, 2015.

[2] V. Madonna, P. Giangrande, and M. Galea, "Electrical Power Generation in Aircraft: Review, Challenges, and Opportunities," *IEEE Transactions on Transportation Electrification,* vol. 4, pp. 646-659, 2018.

[3] X. Roboam, B. Sareni, and A. De Andrade, "More electricity in the air: Toward optimized electrical networks embedded in more-electrical aircraft," *IEEE industrial electronics magazine,* vol. 6, pp. 6-17, 2012.

[4] P. Fang Zheng, A. Joseph, W. Jin, S. Miaosen, C. Lihua, P. Zhiguo*, et al.*, "Z-source inverter for motor drives," *IEEE Transactions on Power Electronics,* vol. 20, pp. 857-863, 2005.

[5] O. Ellabban, H. Abu-Rub, and B. Ge, "A Quasi-Z-Source Direct Matrix Converter Feeding a Vector Controlled Induction Motor Drive," *IEEE Journal of Emerging and Selected Topics in Power Electronics,* vol. 3, pp. 339-348, 2015.

[6] L. W. Parker, "Direct current voltage booster (US2155362A)," United States Patent, 1937.

[7] T. Morita, M. Yanagihara, H. Ishida, M. Hikita, K. Kaibara, H. Matsuo*, et al.*, "650 V 3.1 mΩcm2GaN-based monolithic bidirectional switch using normally-off gate injection transistor," in *2007 IEEE International Electron Devices Meeting*, 2007, pp. 865-868.

[8] E. Lorenzani, F. Immovilli, G. Migliazza, M. Frigieri, C. Bianchini, and M. Davoli, "CSI7: A Modified Three-Phase Current-Source Inverter for Modular Photovoltaic Applications," *IEEE Transactions on Industrial Electronics,* vol. 64, pp. 5449-5459, 2017.

[9] E. Lorenzani, G. Migliazza, and F. Immovilli, "Ground Leakage Current Mitigation for Three-Phase Current Source Inverters," in *2018 IEEE Energy Conversion Congress and Exposition (ECCE)*, 2018, pp. 3694-3699.

[10] G. Buticchi, S. Bozhko, M. Liserre, P. Wheeler, and K. Al-Haddad, "On-Board Microgrids for the More Electric Aircraft—Technology Review," *IEEE Transactions on Industrial Electronics,* vol. 66, pp. 5588-5599, 2019.

[11] J. F. Gieras, "High speed machines," in *Advancements in Electrical Machines 1st edition, ISBN 978-1-4020-9007-3*, ed: Springer, 2008, pp. 81-109.

[12] P. Lindh, I. Petrov, A. Jaatinen-Värri, A. Grönman, M. Martinez-Iturralde, M. Satrústegui*, et al.*, "Direct Liquid Cooling Method Verified With an Axial-Flux Permanent-Magnet Traction Machine Prototype," *IEEE Transactions on Industrial Electronics,* vol. 64, pp. 6086-6095, 2017.

[13] V. Madonna, P. Giangrande, C. Gerada, and M. Galea, "Thermal analysis of fault-tolerant electrical machines for aerospace actuators," *IET Electric Power Applications,* vol. 13, pp. 843-852, 2019.

[14] A. Tenconi, S. Vaschetto, and A. Vigliani, "Electrical Machines for High-Speed Applications: Design Considerations and Tradeoffs," *IEEE Transactions on Industrial Electronics,* vol. 61, pp. 3022-3029, 2014.

[15] A. Binder, T. Schneider, and M. Klohr, "Fixation of buried and surface-mounted magnets in high-speed permanent-magnet synchronous machines," *IEEE Transactions on Industry Applications,* vol. 42, pp. 1031-1037, 2006.

[16] V. Madonna, P. Giangrande, and M. Galea, "Introducing Physics of Failure Considerations in the Electrical Machines Design," presented at the IEMDC 2019 - International Electric Machines & Drives Conference, 2019.

[17] V. Madonna, P. Giangrande, L. Lusuardi, A. Cavallini, C. Gerada, and M. Galea, "Thermal overload and insulation aging of short duty cycle, aerospace motors," *in press on IEEE transactions on Industrial Electronics,* 2019.

[18] A. Al-Timimy, P. Giangrande, M. Degano, Z. Xu, M. Galea, C. Gerada*, et al.*, "Design and Losses Analysis of a High Power Density Machine for Flooded Pump Applications," *IEEE Transactions on Industry Applications,* vol. 54, pp. 3260-3270, 2018.
[19] M. Kaufhold, H. Aninger, M. Berth, J. Speck, and M. Eberhardt, "Electrical stress and failure mechanism of the winding insulation in PWM-inverter-fed low-voltage induction motors," *IEEE Transactions on Industrial Electronics,* vol. 47, pp. 396-402, 2000.
[20] V. Madonna, P. Giangrande, W. Zhao, H. Zhang, C. Gerada, and M. Galea, "On the Design of Partial Discharge-Free Low Voltage Electrical Machines," presented at the IEMDC 2019 - International Electric Machines & Drives Conference, 2019.
[21] M. v. d. Geest, H. Polinder, J. A. Ferreira, and D. Zeilstra, "Current Sharing Analysis of Parallel Strands in Low-Voltage High-Speed Machines," *IEEE Transactions on Industrial Electronics,* vol. 61, pp. 3064-3070, 2014.
[22] "Insight_07 - Electrical Power Systems," UK Aerospace Technology Institute; July 2018.